Spin-Polarized Rb-2 Interacting with Bosonic He Atoms: Potential Energy Surface and Quantum Structures of Small Clusters

ARTICLE *in* THE JOURNAL OF PHYSICAL CHEMISTRY A · MARCH 2012

Impact Factor: 2.69 · DOI: 10.1021/jp3004932 · Source: PubMed

THE JOURNAL OF PHYSICAL CHEMISTRY A

Article

pubs.acs.org/JPCA

Spin-Polarized Rb_2 Interacting with Bosonic He Atoms: Potential Energy Surface and Quantum Structures of Small Clusters

R. Rodríguez-Cantano,[†] David López-Durán,*[,†] T. González-Lezana,[†] G. Delgado-Barrio,[†] P. Villarreal,[†] E. Yurtsever,[‡] and F. A. Gianturco[§]

[†]Instituto de Física Fundamental, IFF-CSIC, Serrano 123, 28006 Madrid, Spain

[‡]Department of Chemistry, Koç University, RumelifeneriYolu, 34450 Sariyer, Istanbul, Turkey

[§]Department of Chemistry and CNISM, University of Rome La Sapienza, Piazzale A. Moro 5, 00185 Rome, Italy

ABSTRACT: A new full-dimension potential energy surface of the three-body He−$Rb_2(^3\Sigma_u^+)$ complex and a quantum study of small $(^4He)_N$−$Rb_2(^3\Sigma_u^+)$ clusters, $1 \le N \le 4$, are presented. We have accurately fitted the ab initio points of the interaction to an analytical form and addressed the dopant's vibration, which is found to be negligible. A Variational approach and a Diffusion Monte Carlo technique have been applied to yield energy and geometric properties of the selected species. Our quantum structure calculations show a transition in the arrangements of the helium atoms from $N = 2$, where they tend to be separated across the diatomic bond, to $N = 4$, in which a closer packing of the rare gas particles is reached, guided by the dominance of the He−He potential over the weaker interaction of the latter adatoms with the doping dimer. The deepest well of the He−Rb_2 interaction is placed at the T-shape configuration, a feature which causes the dopant to be located as parallel to the helium "minidroplet". Our results are shown to agree with previous findings on this and on similar systems.

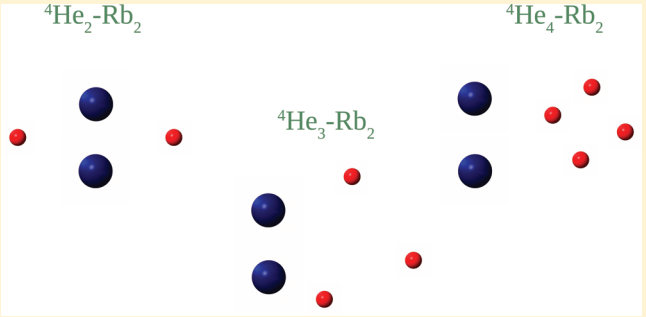

1. INTRODUCTION

The use of nanodroplets of ^4He and/or ^3He of different sizes has been proven over the years to constitute an ideal spectroscopic environment where nonhomogeneous quantum systems can be studied in detail and shown to have properties which are different from those provided by a thin film or a bulk liquid. Thus, these nanodrops create a medium that very efficiently acts as a "quantum matrix", where it becomes possible to store a broad variety of molecular dopants, neutral or charged, which can in turn be investigated by electronic or IR spectroscopy.[1−4]

The success of such probing also comes from the very weak perturbation caused by the solvent He atoms which are able to gently adapt themselves in the vicinity of the molecular dopant. As a consequence, they create a unique and often structured geometric configuration of their aggregates and a very flexible low-T solvent (about 0.5 K for bosonic droplets) which allows the detailed study of even fairly complex systems.[5−9]

The solvation process of an atomic or molecular impurity in helium drops depends on the competition between two different interaction networks: He−impurity and He−He. If the former dominates over the latter, the dopant is likely to penetrate the rare gas cluster, while if the contrary occurs, then it tends to reside outside it. Attraction between any two helium atoms is indeed very weak (only ∼8 cm^{-1}) due to the Pauli repulsion and thus weaker than most of the He−dopant interactions. However, if one finds a doping species exhibiting an even larger Pauli repulsion, then the He−impurity potentials will be smaller than those between adatoms: this is the case of the alkali atoms.[10] Their dimers in the triplet electronic state behave in the same way and have been extensively studied by the groups of Ernst and Stienkemeier: predictions for the observation of KRb spectra under cold conditions,[11] Helium Nanodroplet Isolation (HENDI) experiments applied to Na_2[12] or more up-to-date articles like the reinvestigation of the $Rb_2(2)^3\Pi_g$−$a^3\Sigma_u^+$ band,[13] and wave packet dynamics of alkali dimers,[14] for instance. The general conclusion is that the diatom is placed in a dimple on the surface of the helium nanodroplet, which causes slight modifications in the spectroscopic properties of the impurity.[15]

The above situation poses to theoreticians a substantial challenge for reproducing such findings and to tackle the particular problem where the doping impurity is known to very likely reside outside the helium subcomplex. In an earlier study by Bovino et al.,[16] they carried out Diffusion Monte Carlo (DMC) calculations which demostrated that Li_2 dimers, singlet and triplet species, remain on the surface of small helium clusters, containing up to 30 particles, in either a perpendicular/parallel arrangement with respect to the rare gas partner depending on the $^1\Sigma/^3\Sigma$ spin state. Later on, our group published a new Potential Energy Surface (PES) for the three-body complex He−$Cs_2(^3\Sigma_u^+)$,[17] modeling the interaction

Received: January 16, 2012
Revised: February 9, 2012
Published: February 9, 2012

through a very simple analytical form, allowing Path Integral Monte Carlo (PIMC)[18] and DMC[19] calculations for $(^4He)_N$–$Cs_2(^3\Sigma_u^+)$ complexes, $1 \le N \le 30$, with the same qualitative result as those of ref 16, i.e., the segregation of the guest molecule with respect to the pure He moiety as well as the appearance of a diffuse shell-like structure (see also refs 20–24 for other studies with Br_2 and ICl). Recently, Guillon et al. have presented a PES for the He–$Rb_2(^3\Sigma_u^+)$ system and carried out DMC and PIMC calculations on $(^4He)_N$–$Rb_2(^3\Sigma_u^+)$ clusters.[25] They have interpolated their 108 ab initio points through a certain kind of reproducing kernel Hilbert spaces (RKHS) method[26] and obtained a 2D potential function given in terms of distance-like and angle-like reproducing kernels.[26] Also in this case the Rb_2 remains isolated with respect to the host adatoms. To continue the analysis of such very weakly bound many-particle complexes, we therefore report here a new He–$Rb_2(^3\Sigma_u^+)$ PES and Variational (VAR) (term to be explained better below) and DMC studies of the $(^4He)_N$–$Rb_2(^3\Sigma_u^+)$ clusters, $1 \le N \le 4$; we shall further compare our results with those of Guillon et al.[25] Both PESs are very similar, but our simple model makes the dynamical calculations extremely fast, reducing substantially the computational effort. As done in that article,[25] the rotation of the Rb_2 molecule has been included also in our work, while additionally we have addressed the vibrational degree of freedom of the dimer that we shall show can be ignored in the present calculations. Due to the similarities between the He–$Cs_2(^3\Sigma_u^+)$ and He–$Rb_2(^3\Sigma_u^+)$ PESs, as also discussed below, one can expect the occurrence of similar general features, which would then confirm the earlier findings on both types of systems.[18,19]

The paper is organized as follows: in Section 2 we describe the new He–$Rb_2(^3\Sigma_u^+)$ PES, while Section 3 summarizes the two theoretical frameworks. In Section 4 the numerical details can be found, while present results and conclusions are given in Sections 5 and 6, respectively.

2. COMPUTED INTERACTION

2.1. Ab Initio Calculations. We use Jacobi coordinates (r,R,θ) to describe the 3D PES of the He–$Rb_2(^3\Sigma_u^+)$ complex $W(r,R,\theta)$, where **r** is the vector joining the two atoms of the dimer ($r \equiv |\mathbf{r}|$); **R** is that of the He atom with respect to the center of mass of the Rb_2 ($R \equiv |\mathbf{R}|$); and θ is the angle between **R** and **r**.

For nine values of r (5.45, 5.60, 5.80, 6.00, 6.35, 6.80, 7.25, 8.00, and 10.00 Å), angles are incremented by 10 degrees from 0° to 90° and distances extended out to 20 Å, using different spacings between R values depending on orientation. The total number of computed points was ∼7000. All ab initio calculations are performed with the Gaussian03 program,[27] using the spin-restricted single and double excitation coupled cluster method with perturbative triples [RCCSD(T)] correlating only the valence electrons. Different choices of basis set expansions were implemented and tested before carrying out the final calculations. The potential curve of the Rb_2 molecular partner was generated by selecting six different basis sets and effective core potentials (ECPs) from different groups within the CCSD(T) approach: the LANL2DZ,[28] the CRENBL,[29] and four balanced basis sets of polarized split valence, triple-zeta valence, and quadruple-zeta valence quality of Wiegend and Ahlrichs.[30] In Table 1 we present, for the isolated dimer, the values of r_{eq} (the equilibrium distance) and of D_e (the well-depth), obtained using the above approach, together with previous estimates of those magnitudes.

Table 1. Equilibrium Distance, r_{eq}, and Well-Depth, D_e, Obtained through the Use of Different ECPs for the Rubidium Dimer[a]

this work	r_{eq} (Å)	D_e (cm^{-1})
LANL2DZ[28]	6.95	125.00
CRENBL[29]	6.70	150.69
def2-SVP[30]	6.70	142.62
def2-TZVP[30]	6.35	194.37
def2-TZVPP[30]	6.35	196.80
def2-QZVP[30]	6.35	196.14
Expt. Beser et al.[31]	6.069	241.45
Soldán B basis[32]	6.118	224.8
Soldán C basis[32]	6.102	229.6

[a]Earlier reported values of these magnitudes are also included.

The most recent experiments on the dimer[31] report values of 6.069 Å and 241.45 cm^{-1}, in accordance with recent theoretical estimates.[32] To carry out further three-body calculations keeping the computational effort within acceptable limits, we selected the def2-TZVP[30] basis set, which uses the ECP28MWB pseudopotential.[33] The first two levels supported by this potential were found to be at $E_0 = -188.289$ and $E_1 = -176.372$ cm^{-1}; i.e., there is a vibrational spacing of 11.917 cm^{-1}, and the corresponding wave functions were then used to obtain averaged values $\overline{r}_v = \langle v|r|v\rangle$, $v = 0,1$, and the $\overline{r}_{01} = \langle v = 0|r|v = 1\rangle$ nondiagonal term, reaching values (Å) of $\overline{r}_0 = 6.39$, $\overline{r}_1 = 6.46$, and $\overline{r}_{01} = 0.18$, respectively. As will be shown below, the small values of the difference $\overline{r}_0 - r_{eq} = 0.04$ Å and $\overline{r}_{01}$, together with the weakness of the He–Rb_2 interaction as compared with the vibrational diatomic spacing mentioned above, make largely negligible the difference between considering the rubidium dimer as a rigid rotor, with bond length fixed at r_{eq} within the complex, or to account for its vibrational content at $v = 0$.

In spite of the fact that our results for the dimer are still not very precise, one should however note that this small-core calculation already includes two electrons from the 4s level, six electrons from the 4p level, plus one more electron from the 5s level, i.e., nine electrons for each rubidium atom. This particular choice allows for an explicit treatment of core–valence electron correlation in subsequent calculations and suffices for a correct description of the He–Rb_2 interaction:[17,32] adding 2 electrons from He a total of 20 electrons is explicitely considered.

The basis set for the He atom was also varied from cc-pVQZ, to cc-pV5Z, to aug-cc-pV5Z. In this way, the interaction energies using the supermolecular approach, $\Delta E = E_{HeRb_2} - E_{He}^{BSSE} - E_{Rb_2}^{BSSE}$, were obtained. The best choice, including the BSSE correction,[34] turned out to be the aug-cc-pVQZ in terms of strength of the interaction and feasibility of computational times, producing variations of the minimum values of the attractive well which are very close to those given by the aug-cc-pV5Z basis used in ref 25. The ab initio full 3D PES is available on request from the authors.

2.2. Analytical Representation of the Potential Energy Surface. To represent the PES for the $HeRb_2$ complex in a similar way to what was done for the $HeCs_2$ system,[17] we used a full analytical functional form to fit the CCSD(T) ab initio points. Keeping the diatomic bond length at its equilibrium distance $r_{eq} = 6.35$ Å, we decided first to build a 2D function $W(r_{eq},R,\theta)$, within a small region of energy (below 5 cm^{-1}), by assuming an addition of the two angle-dependent He–Rb

dx.doi.org/10.1021/jp3004932 | J. Phys. Chem. A 2012, 116, 2394–2404

interactions, each of them described by a Lennard-Jones function, i.e.

$$W(r_{eq}, R, \theta) \equiv V(\tilde{R}_1, \theta) + V(\tilde{R}_2, \theta) \quad (1)$$

with $\tilde{R}_i$ being the distance from the helium to the ith rubidium atom and

$$V(x, \theta) = d(\theta)\left[\left(\frac{\bar{x}(\theta)}{x}\right)^{12} - 2\left(\frac{\bar{x}(\theta)}{x}\right)^{6}\right] \quad (2)$$

$d(\theta)$ is the well depth, and $\bar{x}(\theta)$ is the equilibrium distance at a fixed orientation θ. When $\theta = 0$, one realizes that such an addition chiefly reduces to the interaction of He with the nearest Rb atom. A cubic spline fitting to the ab initio points presents a minimum of -0.863 cm^{-1} at $R = 10.801$ Å: the nearest Rb atom is here at a distance of $10.801 - 0.5 \times r_{eq} = 7.63$ Å. Starting with these parameters, a nonlinear square fit produces values of $d = 0.7987$ cm^{-1} and $\bar{x} = 7.6044$ Å. For the perpendicular orientation, the cubic spline fit to the ab initio points presents a minimum of -2.4193 cm^{-1} at 6.355 Å. Using simple geometrical arguments, one thus gets initial values to carry out a nonlinear fit and arrives at values of $d = 1.1730$ cm^{-1} and $\bar{x} = 7.096$ Å for this arrangement. We then assume a two-parameter dependence of these coefficients on the orientation angle

$$d(\theta) = d(0) + [d(\pi/2) - d(0)]\sin^{2\alpha}(\theta) \quad (3)$$

$$\bar{x}(\theta) = \bar{x}(0) + [\bar{x}(\pi/2) - \bar{x}(0)]\sin^{2\beta}(\theta) \quad (4)$$

Simple inspection of the different angular curves reveals that there is a slower variation of them when increasing θ from the linear arrangement than when one approaches the latter from the perpendicular orientation, the behavior being more marked for the well depths than for the equilibrium values. This suggests in eqs 3 and 4 to choose a larger value for the α parameter than for β. The final fit to the ab initio points at the 10 different orientations produces values of $\alpha = 15.214$ and $\beta = 6.173$ for energies below 5 cm^{-1}. Figure 1 depicts $W(r_{eq},R,\theta)$ obtained

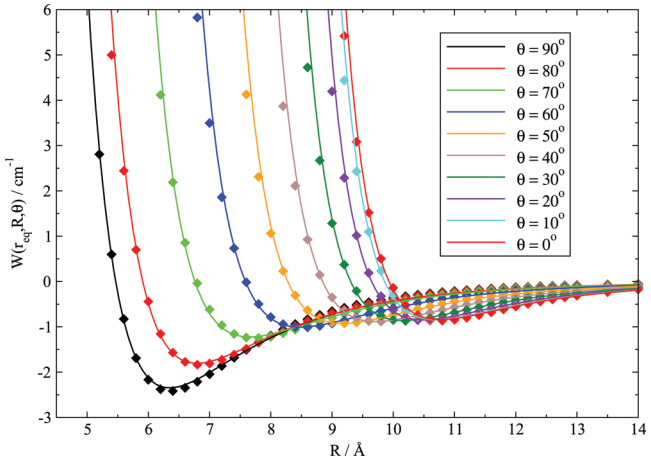

Figure 1. Analytical fitting (lines) and ab initio points (diamonds) of the He−($^3\Sigma_u^+$)Rb_2 PES (see text for details).

using the procedure outlined above, together with the ab initio data, for $\theta = 0,10, \ldots, 90°$: taking into account the simplicity of the model proposed, the agreement is really good. Note that all potential curves coincide for large enough R, showing the correct behavior as $-(1/R^6)$.

The energies ΔE corresponding to the (R,θ) raw points, the analytical fit $W(r_{eq},R,\theta)$, and their differences are collected for the minimum energy position at each θ in Table 2. The partial

Table 2. Interaction Energies and Analytical Potential Values at Selected Orientations, Together with Their Differences and Partial Root Mean Square Errors[a]

(θ, R)	ΔE	$W(r_{eq},\theta,R)$	$\Delta E - W(r_{eq},\theta,R)$	rms
(0,10.80)	−0.843	−0.839	−0.004	0.065
(10,10.80)	−0.859	−0.837	−0.022	0.137
(20,10.60)	−0.860	−0.842	−0.018	0.132
(30,10.20)	−0.868	−0.860	−0.008	0.184
(40,9.80)	−0.883	−0.880	−0.0003	0.154
(50,9.20)	−0.923	−0.925	+0.002	0.190
(60,8.60)	−1.011	−0.999	−0.012	0.113
(70,7.80)	−1.244	−1.211	−0.033	0.088
(80,6.80)	−1.836	−1.804	−0.032	0.126
(90,6.40)	−2.416	−2.342	−0.074	0.045

[a]Energies are in cm^{-1}, angles in degrees, and distances in Å. See text for further details.

standard deviation or root-mean-square (rms) error at each orientation, considering the potential energies below 5 cm^{-1}, is also included. The total rms error is 0.129 cm^{-1}, an error which decreases to 0.029 (0.024) cm^{-1} for energies below 2 (0.1) cm^{-1}, showing that the largest errors come from the repulsive portion of the surface, while the region of the well (which is assumed to be of major importance in the calculation of bound states) is properly described.

Figure 2 shows a contour plot of the analytical 2D surface $W(r_{eq},R,\theta)$ to give a pictorial view of the very marked

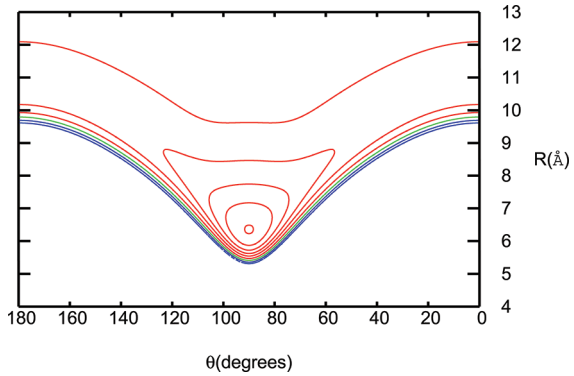

Figure 2. Contour plot of the He−($^3\Sigma_u$)Rb_2 PES. Isolines (cm^{-1}) are plotted from −2.32 at intervals of 0.45 up to −0.52 (red lines), and at 0 (green line), 0.5, and 1 (blue lines).

shallowness of the present interaction. It is worth pointing out that the present plot is actually close to that reported in ref 25.

We turn now to the issue of the diatom's vibration. Taking advantage of the analytical form of the 2D surface $W(r_{eq},R,\theta)$ and the small value of $\bar{r}_0 - r_{eq}$ (= 0.04 Å), we consider a Taylor expansion of such interaction around the equilibrium distance r_{eq} of the dimer

$$\langle 0|W(r, R, \theta)|0\rangle \approx W(r_{eq}, R, \theta) + (\bar{r}_0 - r_{eq})\left.\frac{\partial W}{\partial r}\right|_{r_{eq}} \quad (5)$$

dx.doi.org/10.1021/jp3004932 | J. Phys. Chem. A 2012, 116, 2394−2404

in which terms up to only first order have been retained. Furthermore, one can estimate the coupling with the $v = 1$ state of the Rb_2 by resorting to an analytical diagonalization of the following 2 × 2 matrix

$$\begin{pmatrix} W(r_{eq}, R, \theta) + (\bar{r}_0 - r_{eq})\left.\frac{\partial W}{\partial r}\right|_{r_{eq}} & \bar{r}_{01}\left.\frac{\partial W}{\partial r}\right|_{r_{eq}} \\ \bar{r}_{01}\left.\frac{\partial W}{\partial r}\right|_{r_{eq}} & E_1 - E_0 + W(r_{eq}, R, \theta) + (\bar{r}_1 - r_{eq})\left.\frac{\partial W}{\partial r}\right|_{r_{eq}} \end{pmatrix} \quad (6)$$

Eventually, due to the small value of $\bar{r}_{01}$ and the weakness of the He−Rb_2 potential as compared with the vibrational diatomic spacing $E_1 - E_0$, the lowest eigenvalue $W_0(R,\theta)$ results to be very close to the 2D surface $W(r_{eq},R,\theta)$, making it indifferent to consider the rubidium dimer either as a rigid rotor, with bond length fixed at r_{eq}, or to account for its vibration. $W_0(R,\theta)$, $W(r_{eq},R,\theta)$, and their differences at the minimum energy point for selected orientations are shown in Table 3. The rms error, considering potential energies below 5 cm^{-1}, is also included. The total rms error is of 0.025 cm^{-1}, lower than that corresponding to the analytical 2D fit of the ab initio points.

Table 3. Lowest Eigenvalues $W_0(R,\theta)$ at the Minima of Selected Configurations Which Account for Dimer Vibration and Analytical Potential $W(R,r_{eq},\theta)$, and Their Differences, Together with the rms Errors[a]

(θ, R)	$W_0(R,\theta)$	$W(r_{eq},R,\theta)$	$W_0(R,\theta) - W(r_{eq},R,\theta)$	rms
(0,10.76)	−0.840	−0.839	−0.001	0.027
(30,10.15)	−0.861	−0.860	−0.001	0.020
(60,8.48)	−1.007	−1.005	−0.002	0.004
(90,6.36)	−2.346	−2.345	−0.001	0.035

[a]Energies are in cm^{-1}, angles in degrees, and distances in Å. See text for details.

3. THEORETICAL FRAMEWORKS

3.1. Variational Treatment. The Hamiltonian for the $HeRb_2$ system can be written in Jacobi coordinates as[35,36]

$$H = -\frac{\hbar^2}{2\mu_{Rb_2}}\nabla^2_{\mathbf{r}} + U_{Rb_2}(r) - \frac{\hbar^2}{2\mu}\nabla^2_{\mathbf{R}} + W(\mathbf{R}) \quad (7)$$

μ_{Rb_2} is the Rb−Rb reduced mass; μ is the He−Rb_2 reduced mass; and $U_{Rb_2}(r)$ is the intramolecular Rb−Rb potential. The doping dimer is treated in this work as a $^1\Sigma$ rigid rotor at its equilibrium distance, r_{eq}: the spin effects are neglected,[17,37] its Hamiltonian reduces to only the kinetic term ($U_{Rb_2}(r) = 0$), and the He−impurity interaction is represented as $W(\mathbf{R})$, where the dependence in the r_{eq} parameter has been dropped and $\mathbf{R} \equiv (R,\theta)$. The vectors $\mathbf{r}$ and $\mathbf{R}$ have associated to them the angular momentum vectors $\mathbf{j}$ and $\mathbf{l}$, respectively, yielding the total angular momentum vector $\mathbf{J} = \mathbf{j} + \mathbf{l}$.

In a body-fixed (BF) frame, with the Z^{BF} axis parallel to $\mathbf{R}$, we have considered the next set of wave functions

$$\Phi^{JM}_{n_1 j\Omega}(\hat{\mathbf{r}}, \mathbf{R}) = f_n(R) W^{JM}_{j\Omega}(\hat{\mathbf{r}}, \hat{\mathbf{R}}) \quad (8)$$

f_n are radial functions associated with the He−Rb_2 stretching motion, numerically obtained when searching for the ground-state energy level, E_k, of a set of Schrödinger equations at different orientations $\{\theta_k\}_{k=1,K}$

$$\left\{-\frac{\hbar^2}{2\mu}\frac{\partial^2}{\partial R^2} + W(R;\theta_k)\right\}\phi(R;\theta_k) = E_k\phi(R;\theta_k) \quad (9)$$

The eigenfunctions $\phi(R;\theta_k)$ are further orthogonalized through a Schmidt procedure, leading to an orthonormal set of $\{f(R)\}_{n=1,K}$ functions. $W^{JM}_{j\Omega}$ are the angular functions that depend on unitary vectors $\hat{\mathbf{r}}/\hat{\mathbf{R}}$ in the direction of $\mathbf{r}/\mathbf{R}$, with $\hat{\mathbf{r}} \equiv (\theta,\phi)$ being the orientation in the BF frame and $\hat{\mathbf{R}} \equiv (\theta_R,\phi_R)$ the orientation with respect to a space-fixed (SF) frame. A symmetry-adapted basis set composed of functions of eq 8 is in turn employed to expand the total wave function, taking into account the relevant symmetry operators of the system: total inversion $\mathcal{E}^*$ and exchange of diatomic nuclei for homonuclear impurities, $\mathcal{P}_d$.[38,39] Finally, the Hamiltonian matrix is diagonalized by using standard routines.[40]

For the case of the complex He_2Rb_2, its Hamiltonian can be expressed in satellite coordinates with respect to the center of mass of the Rb_2 dopant as[38]

$$H = -\frac{\hbar^2}{2\mu_{Rb_2}}\nabla^2_{\mathbf{r}} + \sum_{i=1}^{2}\left(-\frac{\hbar^2}{2\mu}\nabla^2_i + W(\mathbf{R}_i)\right) - \frac{\hbar^2}{2m_{Rb}}\nabla_1\cdot\nabla_2 + V(|\mathbf{R}_1 - \mathbf{R}_2|) \quad (10)$$

m_{Rb} is the rubidium mass; $\mathbf{R}_i$ are the coordinates of the two rare gas atoms with respect to the center of mass of the Rb_2; and $V(|\mathbf{R}_1 - \mathbf{R}_2|)$ is the potential between the two solvent adatoms.[38]

If $\mathbf{l}_i$ is the helium orbital angular momentum associated with the ith helium atom, l_i its corresponding quantum number, and n_i that related with the He−impurity vibration, we can collect them in a more general index, $\{q_i\} \equiv \{l_i,n_i\}$, and express the total wave function in the Z^{BF} axis by the following basis set expansion[38]

$$\Phi^{JK}_{q_1q_2L\Omega}(\hat{\mathbf{r}}, \hat{\mathbf{R}}_1, \hat{\mathbf{R}}_2) = f_{n_1}(R_1) f_{n_2}(R_2) W^{JK}_{l_1l_2L\Omega}(\hat{\mathbf{r}}, \hat{\mathbf{R}}_1, \hat{\mathbf{R}}_2) \quad (11)$$

with L the quantum number corresponding to the total orbital angular momentum of any two helium atoms $\mathbf{L} = \mathbf{l}_1 + \mathbf{l}_2$ and $\hat{\mathbf{R}}_k \equiv (\theta_k,\phi_k)$ the orientations of the particles 1 and 2 in the BF frame. The f_k's are the radial functions obtained as before, and $W^{JK}_{l_1l_2L\Omega}(\hat{\mathbf{r}},\hat{\mathbf{R}}_1,\hat{\mathbf{R}}_2)$ are the angular functions. In the case of the four-body complex He_2Rb_2, a new symmetry must be added to the considered group: permutation of He adatoms $\mathcal{P}_{12}$. To finish, standard routines are employed to diagonalize the Hamiltonian matrix.[40]

In the case of He_NRb_2 with $N \geq 3$, an approximate method can be used,[18] and the corresponding results should be considered as mere indications in an attempt to gain some insight into the overall energetics and structure of the larger

dx.doi.org/10.1021/jp3004932 | J. Phys. Chem. A 2012, 116, 2394−2404

complexes. This implies then to consider the following Hamiltonian, instead of that in eq 10

$$H = -\frac{\hbar^2}{2\mu_{Rb_2}}\nabla_{\mathbf{r}}^2 + \frac{N}{2}\sum_{i=1}^{2}\left(-\frac{\hbar^2}{2\mu}\nabla_{\mathbf{i}}^2 + W(\mathbf{R}_i)\right) + \binom{N}{2}V(|\mathbf{R}_1 - \mathbf{R}_2|) \quad (12)$$

where one simplifies the problem into N three-body complexes grouped into $(N/2)$ identical four-body ones and $\binom{N}{2}$ identical He−He interactions.

3.2. Diffusion Monte Carlo approach. The well-known DMC method has been previously explained, and we will not repeat it here (see refs 41−48, for instance). The reader can find details of the implementation employed in this work in refs 16, 17, and 49. If $\mathbf{R} \equiv \{\mathbf{R}_i\}_{i=1}^{N}$collects the coordinates of the N helium atoms, the time-dependent Schrödinger equation is given by

$$i\hbar\frac{\partial\Psi(\mathbf{R}, t)}{\partial t} = (H - E_T)\Psi(\mathbf{R}, t) \quad (13)$$

where we have introduced the arbitrary "reference energy" E_T, which does not influence the final energy results. The total potential is expressed as

$$V_{\text{tot}}(\mathbf{R}) = \sum_{i=1}^{N} W(\mathbf{R}_i) + \sum_{i<j}^{N} V(|\mathbf{R}_i - \mathbf{R}_j|) \quad (14)$$

After introducing the imaginary time $\tau \equiv -it/\hbar$ and the distribution function $f(\mathbf{R},\tau) \equiv \Psi_T(\mathbf{R})\Psi(\mathbf{R},\tau)$, we arrive to the following expression

$$-\frac{\partial f(\mathbf{R}, \tau)}{\partial \tau} = -\sum_i (D_i\nabla_i^2 f(\mathbf{R}, \tau) + D_i\nabla_i[\mathbf{F}(\mathbf{R})f(\mathbf{R}, \tau)]) + [E_L(\mathbf{R}) - E_T)]f(\mathbf{R}, \tau) \quad (15)$$

$\Psi_T(\boldsymbol{R})$ is an analytical trial function which approximates at best the true ground-state wave function, and $D_i \equiv \hbar^2/2\mu$ takes the form of a diffusion coefficient. $\mathbf{F}(\mathbf{R})$ is the quantum force, and $E_L(\boldsymbol{R})$ is the local energy.

The evolution of the N_w replicas or *walkers* of the system in the configurational space through the simulation of a diffusion in the imaginary time leads us to the ground state distribution $f_0 = \Psi_0\Psi_T$ ("mixed estimator").[16,17,49]

The trial wave function of a system formed by an impurity and N helium atoms can be expressed as the product of purely nodeless exponential forms[50]

$$\Psi_T(\mathbf{R}) = \Psi_{\text{He-Imp}}(\mathbf{R})\Psi_{\text{He-He}}(\mathbf{R}) \quad (16)$$

$\Psi_{\text{He-Imp}}(\mathbf{R})$ is the He-dopant part of the wave function

$$\Psi_{\text{He-Imp}}(\mathbf{R}) = \prod_{i=1}^{N}\phi_{\text{He-Imp}}(\mathbf{R}_i) \quad (17)$$

which in this work takes the form

$$\varphi_{\text{He-Imp}}(\mathbf{R}_i) = \varphi_{\text{He-Imp}}(\mathbf{R}_i, \cos\theta_i) = \exp\left\{\frac{p_1 + p_2\cos^2\theta_i}{R_i^3} + \frac{p_3 + p_4\cos^2\theta_i}{R_i^2} + (p_5 + p_6\cos^2\theta_i)\log R_i + (p_7 + p_8\cos^2\theta_i)R_i + p_9 + \log p_{10} + p_{11}\cos^2\theta_i\right\} \quad (18)$$

The homonuclear character of the Rb_2 molecule has been taken into account through the $\cos^2\theta$ factor. The He−He part of the wave function is

$$\Psi_{\text{He-He}}(\mathbf{R}) = \prod_{j<k}^{N(N-1)/2}\exp\{f^{\text{He-He}}(R_{jk})\} \quad (19)$$

R_{jk} is the distance between two helium atoms, and $f^{\text{He-He}}$ are Jastrow functions which include contributions from the Laurent series

$$f^{\text{He-He}}(R_{jk}) = -\left(\left(\frac{p_5}{R_{jk}}\right)^5 + \left(\frac{p_3}{R_{jk}}\right)^3 + \frac{p_1}{R_{jk}} + q_{10}(R_{jk} - R_0) + (q_{30}(R_{jk} - R_0))^3 + (q_{50}(R_{jk} - R_0))^5 + (q_{70}(R_{jk} - R_0))^7\right) \quad (20)$$

4. NUMERICAL DETAILS

4.1. Potential Energy Surface. The overall intracluster potential is assembled as an addition of two-body forces between the components of the droplet, i.e., the He−dimer interaction plus the He−He pair potentials. The PES is expressed as in eq 14, where the Rb−Rb distance is fixed at its equilibrium value of $r_{eq} = 6.35$ Å. The first term in the right-hand side is the sum of N He−diatom interactions W, and the second term is the addition of the $N(N + 1)/2$ He−He potentials, with V being the Aziz−Slaman expression.[51]

4.2. Variational Treatment. The masses used are (amu): $m(\text{Rb}) = 85.4678$ and $m(^4\text{He}) = 4.0026$. 8192 points in the R range [0.1,50] Å and a Numerov procedure have been employed to get the radial wave functions, interpolated with 250 Gaussian points to speed up numerical radial quadratures. Eight angles in the interval $[0,\pi/2]$, equally spaced, have been used, together with $0 \le L \le 10$ (L even) and $0 \le l_i \le 10$. To expand the He−dimer and He−He analytical interactions in Legendre polynomials, 100 Gauss-Legendre points in the $[0,\pi]$ interval were considered. Parities are: inversion $\varepsilon = +1$, exchange of He atoms $\kappa = +1$, and permutation of Rb atoms $\eta = +1$. The energy was converged to within 10^{-3} cm^{-1}.

4.3. Diffusion Monte Carlo Calculations. We have carried out the DMC calculations considering small values of $\Delta\tau$ and large values of N_w within ranges in which the results are in convergence; in particular, $\Delta\tau = 10$ hartree^{-1} and $N_w = 10000$. Geometric distributions, which are not the result of any extrapolation, have been calculated with these values of $\Delta\tau$ and N_w. After a long enough propagation in time, the evolution of the energy has been fitted to a functional form $a + b/t^c$, in which the asymptotic parameter a is the energy of the complex. The coefficients of the He−Rb_2 DMC trial wave function were

dx.doi.org/10.1021/jp3004932 | J. Phys. Chem. A 2012, 116, 2394−2404

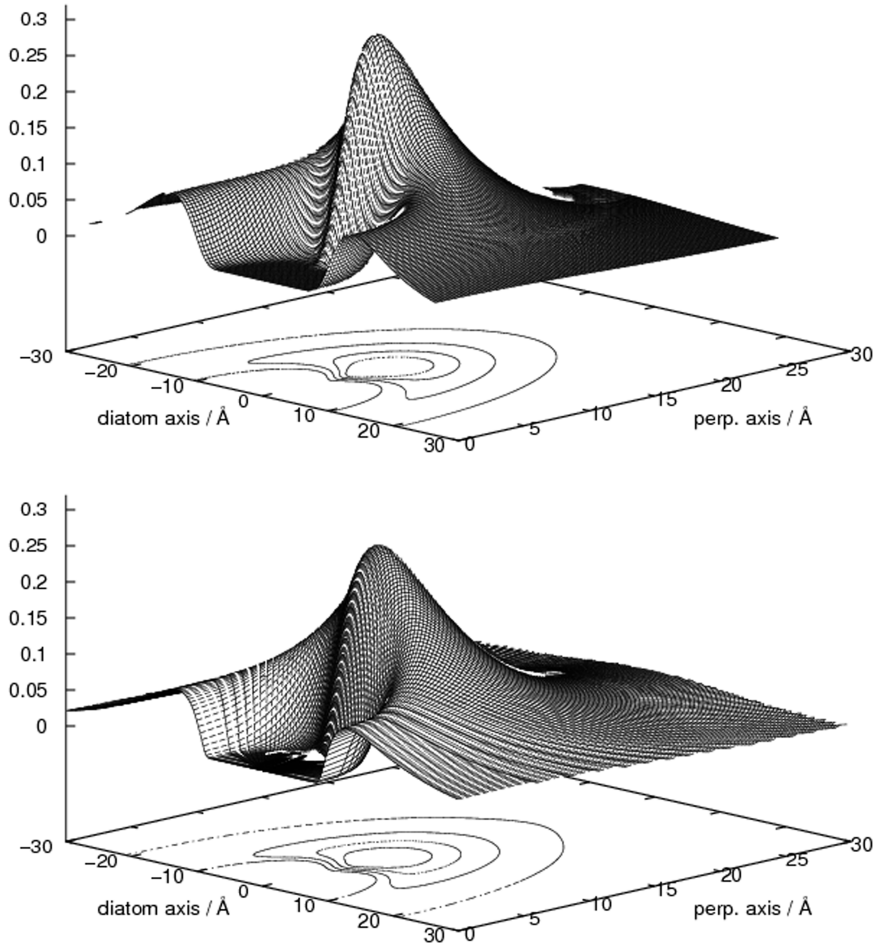

Figure 3. He−Rb_2 VAR wave function (up) and DMC trial wave function (down) normalized to 1, in $Å^{-1}$. Distances in the diatom axis are $X = R \cos \theta$ and in the perpendicular axis $Y = R \sin \theta$, all in Å.

selected by linear squares fitting of the analytical form of eq 18 to the VAR wave function for the $HeRb_2$ species (see Figure 3 and Table 4). The total number of steps was at least $M = 10^6$;

Table 4. Parameters Describing the He−Rb_2 Trial Wave-Function of Equation 18

$p_1 = -1944.8$ bohr^3	$p_7 = -0.013$ bohr^{-1}
$p_2 = -29540.3$ bohr^3	$p_8 = -0.031$ bohr^{-1}
$p_3 = -322.1$ bohr^2	$p_9 = 10.47$ (adim)
$p_4 = 1292.9$ bohr^2	$p_{10} = 0.9$ (adim)
$p_5 = -3.48$ (adim)	$p_{11} = -7.33$ (adim)
$p_6 = 2.27$ (adim)	

the weights that control the population were $w_{min} = 0.5$ and $w_{max} = 2$; and the parameter in the energy reference was $\alpha = 1$.[17]

With respect to the He−He trial wave function in the case of $(^4He)_N$−Rb_2, $N = 2$ and 3, the parameters were selected considering the He−He distance distribution obtained with the VAR approach and are shown in Figure 4 and by Table 5. For $(^4He)_4$−Rb_2 we employed the values given by Lewerenz.[52]

5. RESULTS AND DISCUSSION

5.1. Smallest Complex ($N = 1$). To better analyze and discuss the behavior of the present set of small clusters, it is instructive to compare their very weak forces with the similar ones for the He−$Cs_2(^3\Sigma_u^+)$, which we have recently studied in a series of publications.[17−19] The plots in Figure 5 show the cuts of the two computed PESs at the extreme orientations of the T-shaped and collinear configurations.

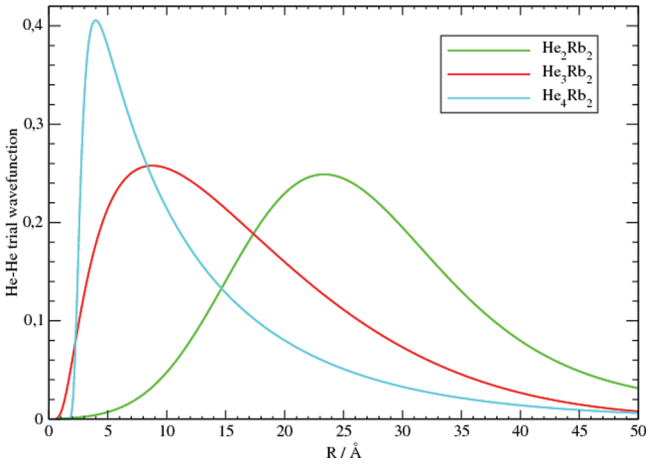

Figure 4. He−He trial wave functions normalized to 1, in $Å^{-1/2}$.

The cuts in the figure clearly indicate the more compact structures, with $R_{min} \sim 6$ Å, for the stronger interacting T-shape complexes, as opposed to $R_{min} \sim 11$ Å for the collinear cases. The two systems, however, are remarkably similar in their interaction potentials, a feature which will become even more evident from our discussion below. One can also see in Figure 5

dx.doi.org/10.1021/jp3004932 | J. Phys. Chem. A 2012, 116, 2394−2404

Table 5. Fitting Parameters for the He−He Trial Wave-Function, for N = 2 and 3 in the Clusters, According to Equation 20

	He_2Rb_2	He_3Rb_2
p_5 (bohr)	0	0.01145
p_3 (bohr)	−1.20798	−0.52862
p_1 (bohr)	2	9
R_0 (bohr)	196	−453.18
q_{10} (bohr^{-1})	−0.08988	−0.00759
q_{30} (bohr^{-1})	0.01881	0.00301
q_{50} (bohr^{-1})	−0.01068	−0.00107
q_{70} (bohr^{-1})	0	0.00226

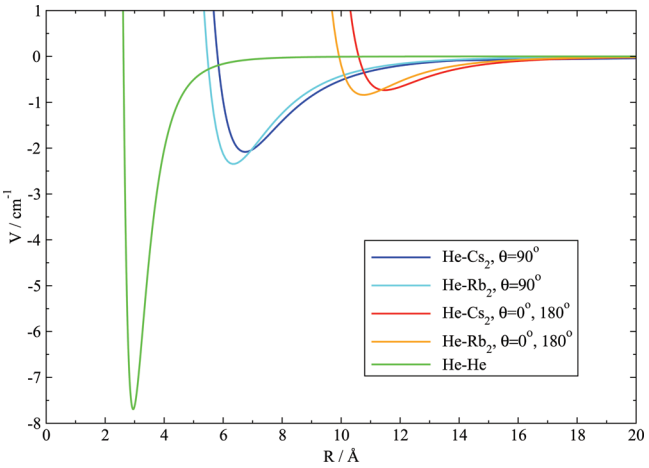

Figure 5. Comparison of the computed PES for the He−Rb_2 and He−Cs_2 complexes, together with the He−He interaction from ref 53. See text for further details.

the relative strength of the He−Rb_2 interaction with that corresponding to the He−He pair. The latter is deeper than the former, and as mentioned before, a packing of the rare gas atoms is most likely to happen, with the ensuing isolation of the dimer. Nevertheless, it constitutes only a propensity rule, and the quantum mechanics calculations must be carried out to confirm this point.

In Table 6, one can see how our VAR and DMC energies for $HeRb_2$ match quite well, with those from ref 25 below them. We have used the three-body complex as a benchmark: (a) to asses the quality of our analytical fit to the calculated ab initio points, (b) to analyze the relevance of the dopant vibration, and (c) to estimate the temperature dependence by including excited rotational states. Regarding the first issue, we applied a RKHS interpolation method[26] in a similar way to what was done in ref 25, although considering radial $q^{2,5}(x_i,x)$, $x = R$ or r, and angular functions $q_1(z_i,z)$, $z = \cos\theta$, reproducing kernels as in ref 53, in 90, 9, and 10 points along R, r, and θ, respectively. The variational ground energy of $HeRb_2$, with the bond length fixed at r_{eq} = 6.35 Å, becomes −0.1150 cm^{-1}, which only differs 0.004 cm^{-1} from the energy calculated via analytical fit, −0.119 cm^{-1}. Regarding the second point, under the RKHS procedure, we repeated the calculation with a dimer elongation of r_0 = 6.39 Å, the averaged diatomic distance in the ground vibrational state. The result is now −0.1145 cm^{-1}, which confirms the negligible contribution of the Rb_2 vibration. Turning now to the third issue, for total inversion and interchange of rubidium atom states

$$\mathcal{E}^* = \mathcal{P}_d = (-1)^J$$

we found, together with the rotationless J = 0 state at −0.119 cm^{-1}, three additional bound levels at −0.100, −0.062, and −0.006 cm^{-1} for J = 1, 2, and 3, respectively. When considering that the rotational diatomic constant is $B_e = 9.8 \times 10^{-3}$ cm^{-1} and that these states above show a main third J_Z component null on the r direction, one concludes that the whole rotation of the complex really corresponds to a rotation of the rubidium diatomics. By now, selecting a Boltzmann averaging[54]

$$\langle E(T)\rangle = \frac{\sum_J (2J+1)E_J e^{-E_J/KT}}{\sum_J (2J+1)e^{-E_J/KT}} \quad (21)$$

we estimate that for very low temperatures the system remains bound. In particular, at a temperature of T = 1/25.6 K one gets an averaged energy of $\langle E(T)\rangle$ = −0.10 cm^{-1}, clearly different from the +0.09 cm^{-1} value reported in ref 25 (belonging to the continuum) and slightly above our results at T = 0 K. Thus, we suggest that the present analysis, within the quality of our selected PES calculations, provides a broad variety of structure indicators for the initial complex system of the dimer with one He atom.

The one-particle distributions $D_1(\cos\theta)$ and $D_1(R)$ are shown in Figure 7 and Figure 8, upper-left panels. Considering the features of the He−Rb_2 potential, a T-shape arrangement for the equilibrium configuration can be anticipated, with a distance from the dimer to the helium atoms of ∼7 Å. From the DMC calculations, an even larger distance would be possible because the maximum of the He-diatom trial wave function is placed at ∼9.3 Å, perpendicular to the dimer. Both VAR and DMC results are seen here to reproduce well this behavior, with $D_1(\cos\theta)$ peaked at 0 ($\theta \sim 90°$) and $D_1(R)$ showing radial maxima around 10−11 Å.

5.2. Larger Complexes. The computed ground state energies of the complexes, He_NRb_2, $1 \le N \le 4$, are summarized in Table 6 and graphically presented by Figure 6, where a

Table 6. VAR and DMC Energies of the He_NRb_2 Complexes, $1 \le N \le 4$, Together with Those from Guillon et al.[25] and Our Estimate at the Same Temperature of T = 1/25.6 K in Reference 25 (Marked with an Asterisk)[a]

	$HeRb_2$	He_2Rb_2	He_3Rb_2	He_4Rb_2
VAR this work	−0.119	−0.218	−0.494	−1.671
DMC this work	−0.1197 ± 0.0003	−0.218 ± 0.001	−0.764 ± 0.006	−1.403 ± 0.004
VAR Guillon et al.	−0.1339			
DMC Guillon et al.	−0.1341 ± 0.0003	−0.3908 ± 0.0006	−0.850 ± 0.004	−1.52 ± 0.01
PIMC Guillon et al.	+0.09 ± 0.04	−0.18 ± 0.01	−0.54 ± 0.03	−1.15 ± 0.03
estimate this work	−0.10			

[a]All units are in cm^{-1}.

dx.doi.org/10.1021/jp3004932 | J. Phys. Chem. A 2012, 116, 2394−2404

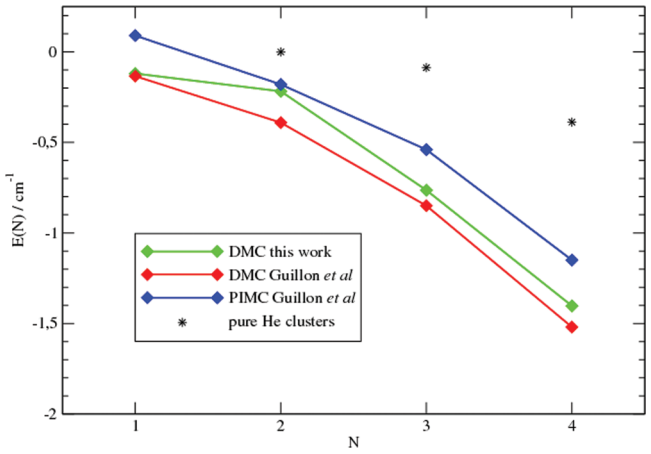

Figure 6. DMC energies for $^4He_NRb_2$ complexes, $1 \leq N \leq 4$, together with those from Guillon et al.[25] The energies of pure He clusters of Lewerenz[52] are also included. All units are in cm^{-1}.

comparison with the values of ref 25 and for pure He aggregates of Lewerenz[52] are also included.

The present results already indicate that all the doped species are bound because their energies are below those for pure ^{4}He complexes. For $N = 2$ our values follow the independent particles model (IPM), and $E(He_2Rb_2) \sim 2 \times E(HeRb_2)$ (correlation energy of the rare gas particles ~0), which makes sense for this case since the two He adatoms of the four-body complex are placed so far from one another, as we shall prove below with their spatial distributions, that their interaction is negligible. The He_3Rb_2 and He_4Rb_2 species do not follow any longer the IPM, and the He−He potential contributions become important. On the whole, the calculations from Guillon et al.[25] give DMC binding energies larger than ours. However, an exhaustive analysis of their values reveals features in disagreement with ours. In the case $N = 1$ let us remind that our estimation of the $HeRb_2$ energy at $T = 1/25.6$ K is -0.10 cm^{-1}, and therefore if this point was included in Figure 6 the three diamonds would be much closer among them. Our smaller binding energy for this complex can be explained in terms of their slightly deeper PES, with a ratio of the potential well minima of 2.59 (Guillon et al.)/2.342 (this work) = 1.1. With regard to $N = 2$ the results of Guillon et al. do not follow the IPM and $E(He_2Rb_2) \sim 3 \times E(HeRb_2)$, in accordance with their description of the He_2Rb_2 system given in ref 25: a packed configuration of the two rare-gas atoms with the resulting large interaction energy. However, it is in contrast with both the same VAR and DMC picture found in this work and other studies with a very similar impurity like Cs_2,[18,19] where a cross-like structure is observed with the ensuing fulfillment of the IPM.

Figure 7 and Figure 8 display the angular and radial one-particle distributions $D_1(\cos\theta)$ and $D_1(R)$, respectively, for the clusters of the present study.

The collocation of the additional helium atoms follows the tendency initially shown by the three-body complex; i.e., it places them in a region around the T-shaped geometry with respect to the diatom. The calculations also show that the larger the cluster, the shorter the distance of the solvent atoms to the diatom: from $R \sim 10$−11 Å for $N = 2$ to $R \sim 8.5$−10 Å for $N = 4$.

One also sees that all distributions become more localyzed, i.e., with narrower and more marked regions of maxima as N increases from 1 to 4, indicating that the systems with the stronger binding energies invariably exhibit a more compact positioning of the He adatoms around the weakly bound dimer. The VAR calculations also show, from the data of Figure 8, that the He atoms are located in closer positions in the subcluster region than in the DMC treatment. Therefore a relationship between the strength of the bond and the compactness of the distributions can be stated, both going through all the sizes studied and when comparing the VAR with the DMC results.

The data of Figure 9 further show the two-particle angular distributions generated by both methods of the present work: VAR and DMC. These distributions refer to the angle γ formed between any two He adatoms with respect to the dopant's center of mass, taken as the vertex of such angle. Note the dramatic change of the distributions when one goes from $N = 2$ to the $N = 3$ and $N = 4$ cases. The four-body cluster could be described as a cross-like structure with the two, lighter adatoms placed away from one another almost along a straight line that cuts the dimer at its midpoint, showing strong delocalization of the He atoms radial positions, as indicated by the two-particle radial distribution given by Figure 10. When one and two more He atoms are added to He_2Rb_2, however, one sees that the

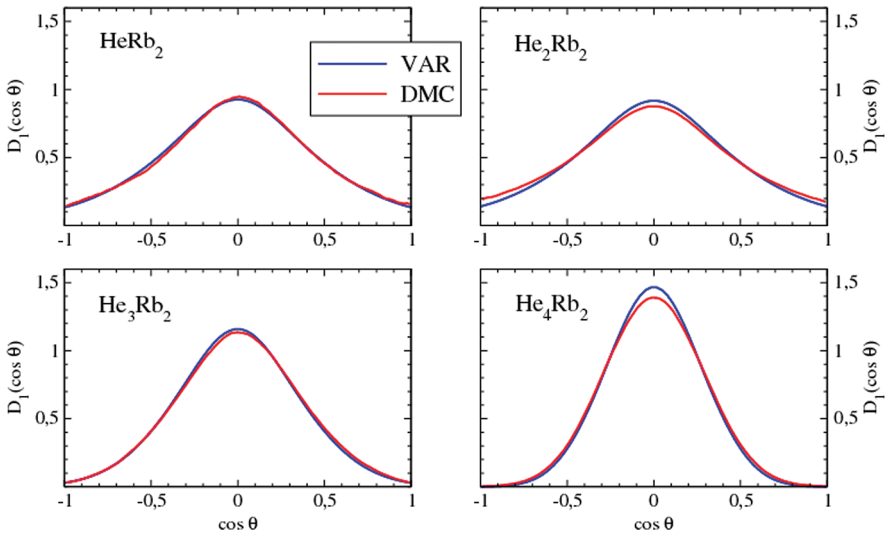

Figure 7. Computed angular distributions, $D_1(\cos\theta)$, for the clusters $^4He_NRb_2$, $1 \leq N \leq 4$. See text for further details.

dx.doi.org/10.1021/jp3004932 | J. Phys. Chem. A 2012, 116, 2394−2404

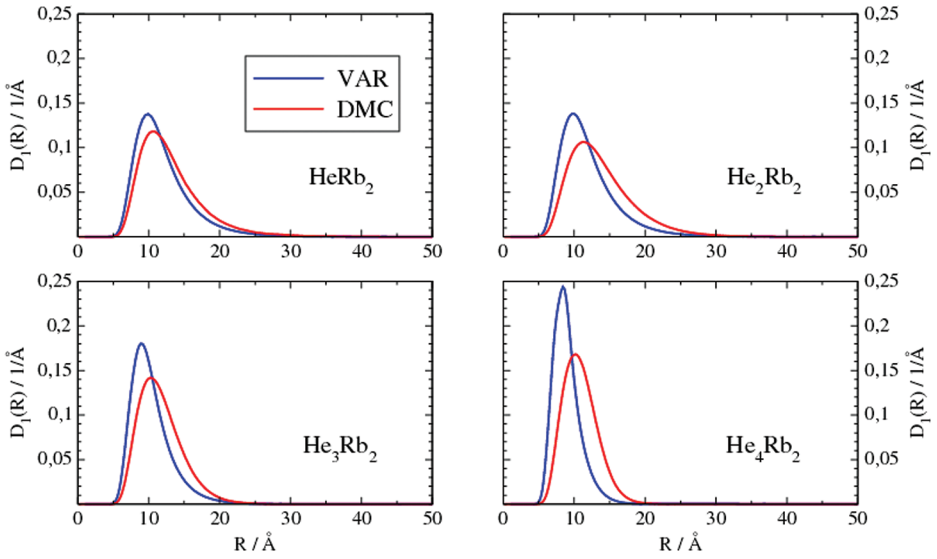

Figure 8. Same as Figure 7 but for the radial distributions, $D_1(R)$, for the clusters $^4He_NRb_2$, $1 \leq N \leq 4$. See text for further details.

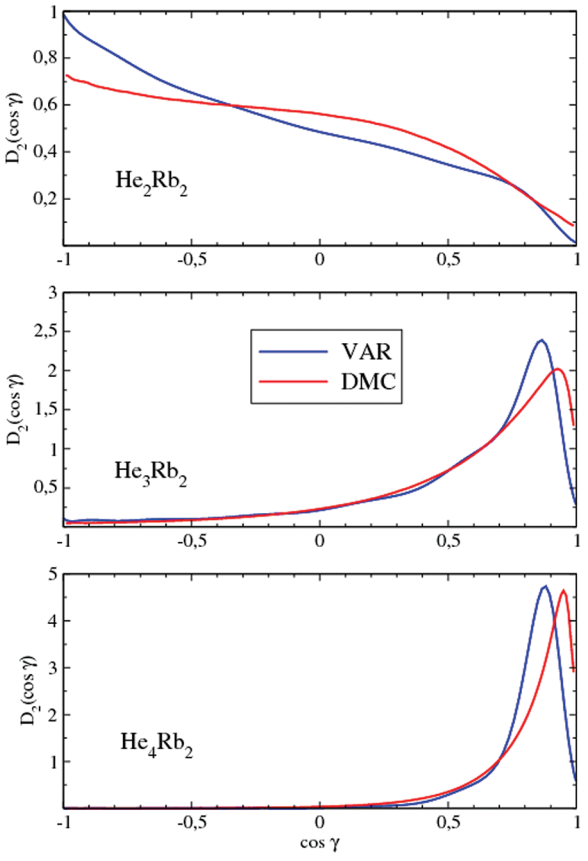

Figure 9. Computed two-particle angular distributions, $D_2(\cos\gamma)$, for the clusters $^4He_NRb_2$, $2 \leq N \leq 4$. See text for further details.

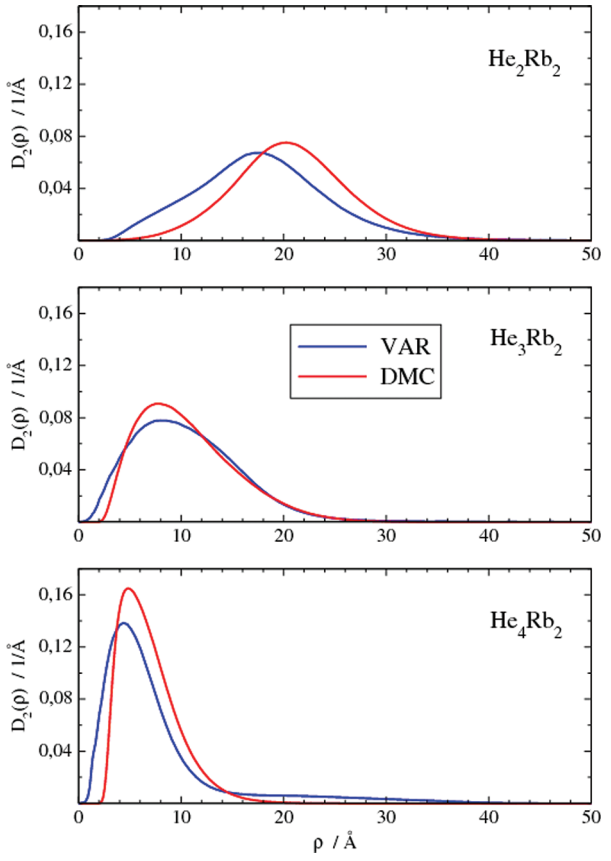

Figure 10. Same as Figure 9 but for the radial distributions, $D_2(\rho)$, for the clusters $^4He_NRb_2$, $2 \leq N \leq 4$. See text for further details.

angular distributions are markedly modified (see Figure 9): the subregion of the solvent atoms acquires greater compactness in space, and all atoms are now "crowding" the interaction region where the strongest He−Rb_2 attaction exists, i.e., around the T-shaped configuration for the complex. As a consequence of this effect, therefore, we see from the data in Figure 9 and Figure 10 that all the He adatoms of the clusters with $N > 2$ exhibit two-particle angle values close to $\gamma \sim 0°$ and relative He−He distances which move down to ~5 Å on the same side of the dopant for $N = 4$. So, as pointed out before, the He−He interactions dominate over the He−dimer one for $N \gtrsim 3$ (clearly seen in He_4Rb_2), while for the four-body complex the latter is the leading potential.

6. CONCLUSIONS

In this work, we have presented a full dimension PES of the He−$Rb_2(^3\Sigma_u^+)$ complex and employed the VAR and DMC procedures to yield energy and geometric results for $(^4He)_N$−$Rb_2(^3\Sigma_u^+)$

dx.doi.org/10.1021/jp3004932 | J. Phys. Chem. A 2012, 116, 2394−2404

clusters, $1 \leq N \leq 4$, with the dimer treated as a rigid rotor at the equilibrium distance and including its rotational Hamiltonian term. The overall PES has been modeled as a sum of pairwise functions which give the interactions between the diatom and each helium atom and those of the helium atoms among themselves. The helium-impurity potential has been obtained from ab initio calculations (discussed in Section 2) and expressed analytically as a pair of Lennard-Jones functions whose terms take into account the anisotropy of the problem. The He−He potential is described through and Aziz−Slaman parametrization.

The main conclusions we arrive to are:

1. The quality of our analytical fit to the raw ab initio points of the He−Rb_2 PES is at least the same as an RKHS interpolation,[26] as done in ref 25.
2. The extremely simple analytical fit makes it possible to carry out Monte Carlo calculations with reasonable computational effort.
3. The vibrational degree of freedom of the Rb_2 can be neglected without loss of accuracy since the interaction energy $W_0(R,\theta)$ is almost identical to the 2D surface $W(r_{eq},R,\theta)$.
4. There is a transition in the species arrangements: from the cross-like structure in He_2Rb_2 to the gathering of the rare gas atoms in a pure subcomplex of helium in He_4Rb_2, with He_3Rb_2 having the role of an intermediate configuration, in accordance with previous works.[16,18]

The study of such small systems has allowed us to attain a detailed description of both the energy and structure parameters as they evolve within a limited set of aggregates: a strong quantum character with marked spatial delocalization. However, all clusters are bound with respect to the $(^4He)_N$ + Rb_2 asymptotes and suggest that the dopant dimer will be sitting outside the complex and parallel to it, as found before in the case of other triplet diatoms.[16,18,19] A more extended study of larger species, using a variety of methods, will be presented elsewhere to further increase our understanding of the larger clusters of very weakly bound members.[55]

AUTHOR INFORMATION

Corresponding Author

*E-mail: davidl@iff.csic.es.

Notes

The authors declare no competing financial interest.

ACKNOWLEDGMENTS

The authors are grateful to the Centro de Cálculo (IFF, CSIC), Centro Técnico de Informática (CTI, CSIC), Centro de Supercomputación de Galicia (CESGA), and CASPUR Computing Consortium for the allocation of computer time. This work has been supported by MICINN, Grants Nos. FIS2010-18132 and FIS2011-29596-C02-01. R.R.-C. and D.L.-D. acknowledge the Spanish programs JAE-PREDOC, grant No. JAE-Pre-2010-01277, and JAE-DOC, Contract Id. E-28-2009-0448699, respectively. The aid of COST Action CM1002 (CODECS) is also appreciated.

REFERENCES

(1) Toennies, J. P.; Vilesov, A. *Annu. Rev. Phys. Chem.* **1998**, *49*, 1.
(2) Toennies, J. P.; Vilesov, A. F.; Whaley, K. B. *Phys. Today* **2001**, *54*, 31.
(3) Toennies, J. P.; Vilesov, A. F. *Angew. Chem., Int. Ed.* **2004**, *43*, 2622.
(4) Stienkemeier, F.; Vilesov, A. F. *J. Chem. Phys.* **2001**, *115*, 10119.
(5) Goyal, S.; Schutt, D. L.; Scoles, G. *Phys. Rev. Lett.* **1992**, *69*, 933.
(6) Ceperley, D. M. *Rev. Mod. Phys.* **1995**, *67*, 279.
(7) Grebenev, S.; Toennies, J. P.; Vilesov, A. *Science* **1998**, *279*, 2083.
(8) Paesani, F.; Gianturco, F. A.; Whaley, K. B. *J. Chem. Phys.* **2001**, *115*, 10225.
(9) Moroni, S.; Baroni, S. *Comput. Phys. Commun.* **2005**, *169*, 404.
(10) Hernando, A.; Barranco, M.; Mayol, R.; Pi, M.; Ancilotto, F.; Bünermann, O.; Stienkemeier, F. *J. Low Temp. Phys.* **2010**, *158*, 105.
(11) Allard, O.; Nagl, J.; Auböck, G.; Callegari, C.; Ernst, W. E. *J. Phys. B* **2006**, *39*, S1169.
(12) Class, P.; Droppelmann, G.; Schulz, C. P.; Mudrich, M.; Stienkemeier, F. *J. Phys. Chem. A* **2007**, *111*, 7537.
(13) Auböck, G.; Aymar, M.; Dulieu, O.; Ernst, W. E. *J. Chem. Phys.* **2010**, *132*, 054304.
(14) Schlesinger, M.; Mudrich, M.; Stienkemeier, F.; Strunz, W. T. *Chem. Phys. Lett.* **2010**, *490*, 245.
(15) Auböck, G.; Nagl, J.; Callegari, C.; Ernst, W. E. *J. Phys. Chem. A* **2007**, *111*, 7404.
(16) Bovino, S.; Coccia, E.; Bodo, E.; López-Durán, D.; Gianturco, F. A. *J. Chem. Phys.* **2009**, *130*, 224903.
(17) Prosmiti, R.; Delgado-Barrio, G.; Villarreal, P.; Yurtsever, E.; Coccia, E.; Gianturco, F. A. *J. Phys. Chem. A* **2009**, *113*, 14718.
(18) Pérez de Tudela, R.; López-Durán, D.; González-Lezana, T.; Delgado-Barrio, G.; Villarreal, P.; Gianturco, F. A.; Yurtsever, E. *J. Phys. Chem. A* **2011**, *115*, 6892.
(19) López-Durán, D.; Pérez de Tudela, R.; Rodríguez-Cantano, R.; González-Lezana, T.; Lara-Castells, M. P.; Delgado-Barrio, G.; Villarreal, P. *Phys. Scr.* **2011**, *84*, 028107.
(20) López-Durán, D.; de Lara-Castells, M. P.; Delgado-Barrio, G.; Villarreal, P.; Di Paola, C.; Gianturco, F. A.; Jellinek, J. *Phys. Rev. Lett.* **2004**, *93*, 053401.
(21) López-Durán, D.; de Lara-Castells, M. P.; Delgado-Barrio, G.; Villarreal, P.; Di Paola, C.; Gianturco, F. A.; Jellinek, J. *J. Chem. Phys.* **2004**, *121*, 2975.
(22) de Lara-Castells, M. P.; López-Durán, D.; Delgado-Barrio, G.; Villarreal, P.; Di Paola, C.; Gianturco, F. A.; Jellinek, J. *Phys. Rev. A* **2005**, *71*, 033203.
(23) Di Paola, C.; Gianturco, F. A.; López-Durán, D.; de Lara-Castells, M. P.; Delgado-Barrio, G.; Villarreal, P.; Jellinek, J. *Chem. Phys. Chem.* **2005**, *6*, 1348.
(24) de Lara-Castells, M. P.; Prosmiti, R.; Delgado-Barrio, G.; López-Durán, D.; Villarreal, P.; Di Paola, C.; Gianturco, F. A.; Jellinek, J. *Phys. Rev. A* **2006**, *74*, 053201.
(25) Guillon, G.; Zanchet, A.; Leino, M.; Viel, A.; Zillich, R. E. *J. Phys. Chem. A* **2011**, *115*, 6918.
(26) Ho, T. S.; Rabitz, H. *J. Chem. Phys.* **1996**, *104*, 2584.
(27) Frisch, M. J.; Trucks, G. W.; Schlegel, H. B.; Scuseria, G. E.; Robb, M. A.; Cheeseman, J. R.; Montgomery Jr, J. A.; Vreven, T.; Kudin, K. N.; Burant, J. C.; et al., *Gaussian03*, Revision B.05; Gaussian, Inc.: Pittsburh, PA, 2003.
(28) Hay, P. J.; Wadt, W. R. *J. Chem. Phys.* **1985**, *82*, 299.
(29) LaJohn, L. A.; Christiansen, P. A.; Ross, R. B.; Atashroo, T.; Ermler, W. C. *J. Chem. Phys.* **1987**, *87*, 2812.
(30) Weigend, F.; Ahlrichs, R. *Phys. Chem. Chem. Phys.* **2005**, *7*, 3297.
(31) Beser, B.; Sovkov, V. B.; Bai, J.; Ahmed, E. H.; Tsai, C. C.; Xie, F.; Li, L.; Ivanov, V. S.; Lyyra, A. M. *J. Chem. Phys.* **2009**, *131*, 094505.
(32) Soldán, P. *J. Chem. Phys.* **2010**, *132*, 234308.
(33) Leininger, T.; Nicklass, A.; Küchle, W.; Stoll, H.; Dolg, M.; Bergner, A. *Chem. Phys. Lett.* **1996**, *255*, 274.
(34) Boys, S. F.; Bernardi, F. *Mol. Phys.* **1970**, *19*, 553.
(35) Beswick, J. A.; Delgado-Barrio, G. *J. Chem. Phys.* **1980**, *73*, 3653.
(36) Gianturco, F. A. *The transfer of molecular energy by collisions*; Springer: Berlín, 1979.
(37) Wernli, M.; Bodo, E.; Gianturco, F. A. *Eur. Phys. J. D* **2007**, *45*, 267.

(38) Villarreal, P.; Roncero, O.; Delgado-Barrio, G. *J. Chem. Phys.* **1994**, *101*, 2217.
(39) Hernández, M. I.; Halberstadt, N.; Sands, W. D.; Janda, K. C. *J. Chem. Phys.* **2000**, *113*, 7252.
(40) Linear algebra package 3.2.1.2009, http://www.netlib.org/lapack/.
(41) Reynolds, P. J.; Ceperley, D. M.; Alder, B. J.; Lester, W. A. Jr *J. Chem. Phys.* **1982**, *77*, 5593.
(42) Ceperley, D. M.; Adler, B. *Science* **1986**, *231*, 555.
(43) Lester, W. A. Jr; Hammond, B. L. *Annu. Rev. Phys. Chem.* **1990**, *41*, 283.
(44) Barnett, R. N.; Reynolds, P. J.; Lester, W. A. Jr *J. Comput. Phys.* **1991**, *96*, 258.
(45) Hammond, L. B.; Lester Jr, W. A.; Reynolds, P. J. *Monte Carlo methods in ab initio quantum chemistry*; World Scientific, Singapore, 1994.
(46) Blume, D.; Lewerenz, M.; Huisken, F.; Kaloudis, M. *J. Chem. Phys.* **1996**, *105*, 8666.
(47) Blume, D. *Phys. Rev. A* **2002**, *66*, 053613.
(48) Hinkle, C. E.; McCoy, A. B. *J. Phys. Chem. Lett.* **2010**, *1*, 562.
(49) Paesani, F.; Gianturco, F. A.; Lewerenz, M.; Toennies, J. P. *J. Chem. Phys.* **1999**, *111*, 6897.
(50) Bodo, E.; Coccia, E.; López-Durán, D.; Gianturco, F. A. *Phys. Scr.* **2007**, *76*, C104.
(51) Aziz, R. A.; Slaman, M. J. *J. Chem. Phys.* **1991**, *94*, 8047.
(52) Lewerenz, M. *J. Chem. Phys.* **1997**, *106*, 4596.
(53) Stoecklin, T.; Voronin, A.; Rayez, J. C. *Phys. Rev. A* **2002**, *66*, 042703.
(54) Pérez de Tudela, R.; Márquez-Mijares, M.; González-Lezana, T.; Roncero, O.; Miret-Artés, S.; Delgado-Barrio, G.; Villarreal, P. *J. Chem. Phys.* **2010**, *132*, 244303.
(55) López-Durán, D.; Rodríguez-Cantano, R.; González-Lezana, T.; Delgado-Barrio, G.; Villarreal, P.; Yurtsever, E.; Gianturco, F. A. *J. Phys.: Condens. Matter* **2012**, *24*, 104014.